A plasmodium falciparum sporozoite's journey: through organs and across CD8+ T-cell challenges

Schuijlenburg, R. van

Chapter 2

Early activation of lung CD8$^+$ T cells after immunization with live *Plasmodium berghei* malaria sporozoites

Roos van Schuijlenburg, Chanel M. Naar, Stefanie van der Wees, Severine C. Chevalley-Maurel, Nikolas Duszenko, Helena M. de Bes-Roeleveld, Eva Iliopoulou, Emma L. Houlder, Fiona J.A Geurten, Els Baalbergen, Meta Roestenberg, Blandine Franke-Fayard

Pathogens and immunity 2025. DOI: 10.20411/pai.v11i1.794

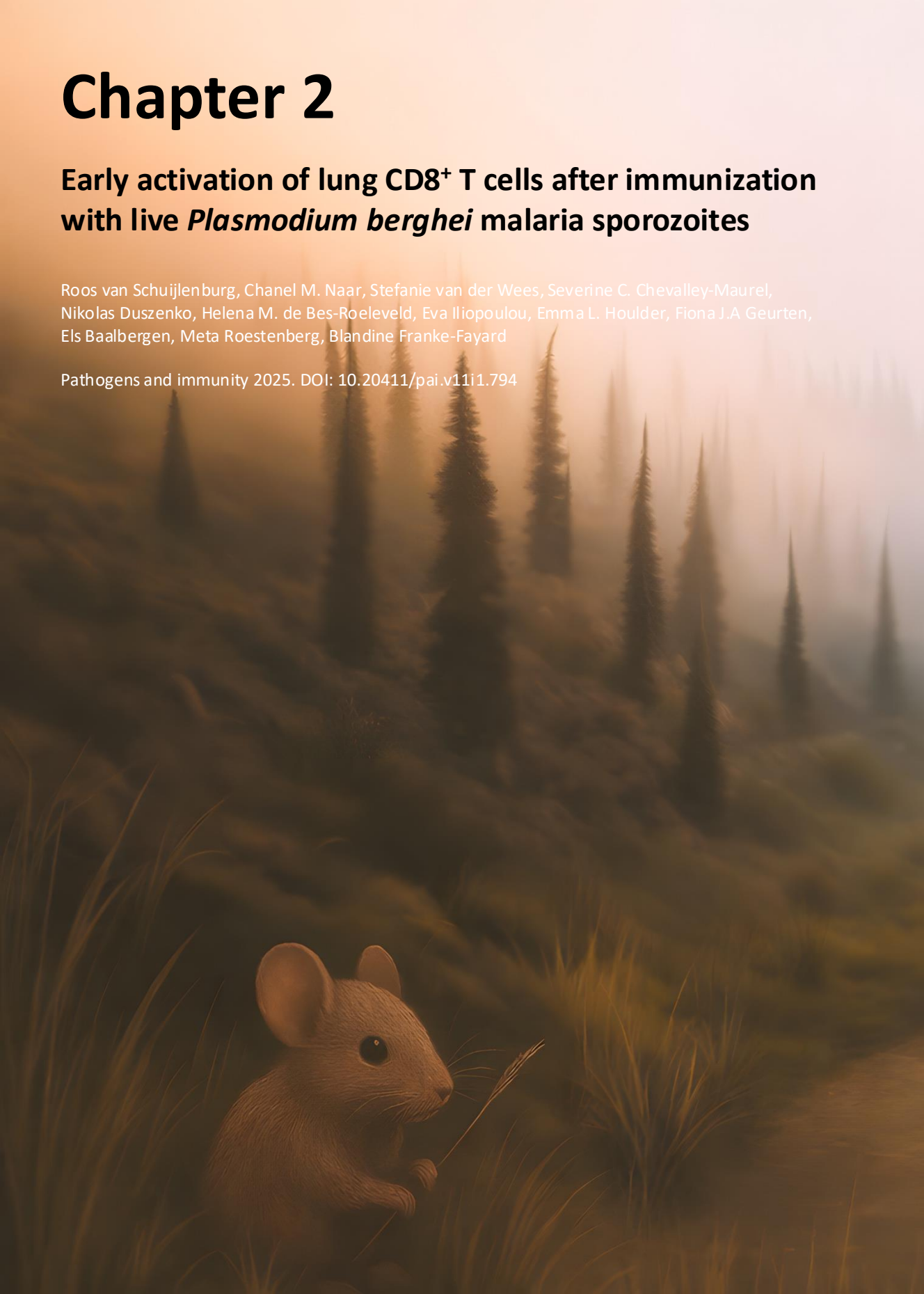

Abstract

Two novel malaria vaccines, RTS,S and R21, mark a significant step forward in malaria research, but eradication demands vaccines with higher efficacy. Recent trials using late-arresting genetically attenuated parasites (LA-GAP) highlight their effectiveness as next-generation vaccines, likely through $CD8^+$ T-cell activation targeting late liver-stage parasites. However, the distribution of LA-GAP-activated T cells in different organs that culminate towards high-level protection in the liver remains unclear. In this study, we aimed to map immune responses in the livers and lungs of mice immunized with LA-GAP, shedding light on the role of different organs in priming T-cell responses towards immunity. Particularly in the lungs we found an impressive increase of $CD8^+$, double negative T cells (5%), γδ (2.5%), effector memory $CD8^+$ T cells (46%), and tissue resident memory $CD8^+$ T cells (3%). These lung T cells are highly activated (expressing CD11c, Ki67, KLRG1) and exhibited 4-fold higher Granzyme A expression and significant TNF^+ cell increases as compared to their liver counterparts (10.2% vs 2.6%). These differences start already at the early 2-day timepoint at which time the lungs show an impressive 10.2% increase in TNF^+ $CD8^+$ T cells, whereas the liver shows a more modest increase of 2.6% of these cells. These findings highlight the lungs as a crucial site for immune priming and T-cell activation, underscoring the need for further investigation of organ-specific responses to fully understand the potential of LA-GAP immunization as a powerful strategy in the fight against malaria.

Introduction

The rollout of 2 novel malaria vaccines (RTS,S and R21) in sub-Saharan Africa in 2024 for children in medium and high-transmission areas marks the success of decades of malaria vaccine research [1]. These circumsporozoite protein (CSP)-based vaccines now provide the much-needed additional tool to control the increasing number of malaria cases. However, to break malaria transmission, vaccines with higher and broader efficacy are urgently needed. Whole sporozoite (SPZ) vaccination approaches can provide such high protective efficacy, as they allow for the induction of cellular immune responses in addition to CSP-targeting antibodies [2, 3]. Whereas antibodies mediate inhibition of *Plasmodium falciparum* (*Pf*) SPZ motility and invasion of the host, cellular mechanisms are thought to be responsible for killing of the ensuing *Pf*-infected liver cells [4, 5]. This is further supported by our recent finding in an experimental medicine trial where we compared the protective efficacy of immunization with early-arresting (24 hours) genetically attenuated whole SPZ with late-arresting (6-7 days) counterparts in healthy malaria-naïve adults. We found that only the late-arresting genetically attenuated parasites (LA-GAP) were able to efficiently induce protective immunity as tested by controlled human malaria infection [6, 7]. These data, combined with the knowledge acquired from animal models that shows protection against malaria relies on $CD8^+$ T cells detecting malaria-infected hepatocytes [8-10], suggest that the activation of $CD8^+$ T cells targeting the late liver stage parasite is a critical mechanism of these highly potent whole SPZ vaccines.

Despite multiple human clinical trials with whole SPZ vaccination approaches, very little is known about T-cell mediated activation and killing of liver stage parasites. Signals of polyfunctional $CD4^+$ T-cell activation and particularly γδ T-cell activation in peripheral mononuclear cells of protected individuals are not very informative of the mechanism of protection, which is presumed to be located specifically in the liver [11, 12]. Given the inaccessibility of the liver in healthy volunteers, very little is known about priming and potentially boosting of liver-stage specific T cells.

However, in animal models, $CD8^+$ T-cell responses after malaria infection have been described in blood, skin, draining lymph nodes, spleen, and liver [13, 14]. The types of immune responses per organ have been found to vary in terms of magnitude and type of responses. For example, skin-based responses are found to be more regulatory with $CD8^+$ T-cell priming occurring mainly through dermal $CD11c^+$ dendritic cells (DCs) in the skin draining lymph nodes [15, 16]. Splenic DCs were also found to prime $CD8^+$ T cells when they encounter SPZ, but the magnitude and durability of the $CD8^+$ T-cell response

may be influenced by the presence of activated $CD4^+$ T cells and γδ T cells [17, 18]. Whereas $CD8^+$ T cells are generally thought to circulate, it is the proportion that becomes tissue-resident memory T cells (Trms) that is thought to be the front line of defense for long-lived immunity induced after whole SPZ immunization [19]. A better understanding of the potential priming and boosting of T-cell responses and the ultimate settling of Trms in different organs is critical to better target the LA-GAP immunogen to the appropriate organs and more efficiently induce protection. As SPZ vaccines are currently injected by direct venous inoculation, we argued that it would be critical to follow the immune activation on the migratory path of SPZ in the blood circulation, traveling through the lungs first before reaching their liver target organ. Interestingly, the role of the lung immune system in LA-GAP immunization has been neglected so far, despite the fact that SPZs, when injected into the blood circulation, must recirculate possibly multiple times through the lungs before arriving at the liver. We thus set out to map the immune responses following SPZ immunization in both lungs and livers of mice immunized with LA-GAP (Figure 1).

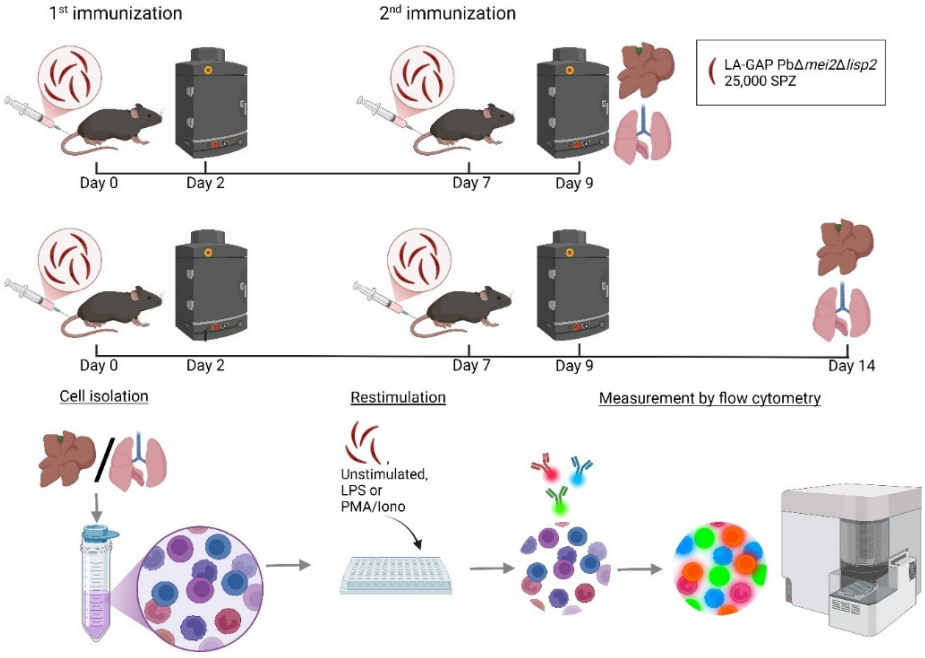

Figure 1. Experimental setup. Timeline of the study protocol. Mice were intravenously immunized with 25,000 *Plasmodium berghei* late-arresting genetically attenuated parasites (LA-GAP) PbΔ*mei2 Δlisp2*, salivary gland extract (SGE), or medium as negative control in C57BL/6J mice, after which liver load was determined, and organs were harvested 2 days post second immunization or 7 days post second immunization. Created with BioRender.com.

Methods

Mosquito Production

Mosquitoes from a colony of *Anopheles stephensi* (line Nijmegen SDA500) were used to obtain SPZs. Larval stages were reared in water trays at a temperature of 28 ± 1°C and a relative humidity of 80%. Adult females were transferred to incubators with a temperature of 26 ± 0.2°C and a relative humidity of 80%. For all the experiments, 3- to 5-day old mosquitoes were used. The *Plasmodium berghei* (Pb)-infected mosquitoes were maintained at 21°C at 80% relative humidity.

Experimental Animals, *P. berghei* Parasite Line

Female OF1 mice and female and male C57BL/6J mice (Charles River Laboratories) of 4 to 6 weeks old were acclimatized for 1 week prior to the experiment. Mice were housed between 4 to 5 mice per cage in ventilated cages with autoclaved aspen woodchip, fun tunnel, wood chew block and nestlets (12:12 hour light-dark cycle; 21 ± 2°C; relative humidity of 55 ± 10%). During the experiment, mice were fed with commercially prepared autoclaved dry rodent diet pellets and water, both available *ad libitum*. All animal experiments were granted with license 11600202216547 by the Competent Authority after advice on ethical evaluation by the Animal Experiments Committee Leiden and were performed in accordance with the Experiments on Animals Act (Wod, 2014), the applicable legislation in the Netherlands in accordance with the European guidelines (EU directive no 2010/63/EU). The study was executed in a licensed establishment for experimental animals.

Mice were euthanized (cardiac puncture under anesthesia) at a parasitemia of 2% to 5% before malaria-associated symptoms occurred. Humane endpoints: the animals' body condition was thoroughly examined daily. Animals were humanely sacrificed if the following defined end points were reached: visible pain (abnormal posture and/or movement), abnormal behavior (isolation, abnormal reaction to stimuli, no food and water intake). No mice were euthanized due to humane endpoints, only one mouse had been excluded due to parasite break-through (explained below).

The LA-GAP Pb*Δmei2Δlisp2* parasite (2900cl3, mutant RMgm-4937; www.pberghei.eu), which is genetically attenuated by the deletion of the meiosis inhibited 2 (*mei2*) and liver-specific protein 2 (*lisp2*) genes [6] was used. Feeding of *Anopheles stephensi* mosquitoes was performed as described previously [20].

***In vivo* Immunization of mice with Pb SPZ**

The study including data acquisition was performed blinded. The study was unblinded after data analysis.

One day prior to immunizations, mice were randomized into 3 or 4 different groups (4-5 mice per group, maximum of 20 mice per experiment). On the day of immunizations, salivary glands (21-23 days post blood meal) of *P. berghei* LA-GAP PbΔ*mei2*Δ*lisp2* (*Pb* SPZ)-infected mosquitoes were dissected in cold RPMI 1640 glutamax (Thermo Fisher). As a control, salivary glands from the same batch of uninfected mosquitoes, hence referred to as salivary gland extract (SGE), were dissected in cold RPMI 1640 glutamax. Immediately after dissection the glands were crushed and homogenized and the total number of *Pb* SPZ was counted. Dead *Pb* SPZs were used as a control, and chemical killing was performed by incubating fresh *Pb* SPZ with 10 µg/mL nucleic acid stain Hoechst (33342, Themofisher) for 30 minutes in a 37°C water bath. Directly after, dead SPZs were washed 5 times with RPMI 1640 glutamax and recounted before use.

Intravenous immunization in the tail vein was performed after warming of the mice under a heat lamp set at 35°C to dilate the veins. For every immunization, 25,000 live or dead *Pb* SPZs were inoculated in 200 µL RPMI 1640 glutamax. SGE and medium were used as controls. For the SGE control, an equal amount of SGE was injected in 200 µL RPMI 1640 glutamax and for the medium control, 200 µl RPMI 1640 glutamax. Second immunizations were given 7 days after the first. All injections were given between 1 PM and 3 PM.

Determination of parasite liver load after first and second immunization by real-time in vivo imaging

After 44 hours post immunization, the parasitic liver load was determined through bioluminescent imaging. Imaging was performed using the IVIS Lumina II Imaging System (Perkin Elmer Life Sciences) [21] 12 minutes after a subcutaneous injection with D-luciferin dissolved in PBS (100 mg/kg; Caliper Life Sciences). Quantitative analysis of bioluminescence of whole bodies was performed by measuring the luminescence signal intensity using the region of interest settings of the Living Image® 4.4 software. Blood-stage breakthroughs were checked at 5 to 6 days post first immunization and second immunization. If any parasites were discovered in the blood, the mice were sacrificed and eliminated from the experiment. This happened to one mouse after the second immunization.

Organ harvesting and processing

Two days or 7 days after the final immunizations, mice were anesthetized via intraperitoneal injection of 10% ketamine (Dechra Pharamceuticals) with 20 mg/mL xylazine (Alfasan). Blood was subsequently collected via retro-orbital puncture and put on ice. The blood was spun down at 4°C. Plasma was collected and stored at -80°C. The liver and lungs were perfused by slowly injecting 20 mL cold PBS via the heart, followed by dissection of the liver and lungs, and placed in sterile RPMI 1640 glutamax on ice.

Livers were processed via mincing with a blade and placed in a 50-ml tube with 20 mL RPMI 1640 glutamax containing 1 mg/mL Collagenase IV (Sigma-Aldrich) and 2,000 U/mL DNase I (Sigma-Aldrich) and incubated for 45 minutes at 37°C, mixing once during incubation. After incubation, tubes were placed on ice and poured through a 100-micron filter (BD) and washed with 20 mL PBS supplemented with 1% Fetal Calf Serum (FCS) and 2.5 mM ethylenediamine tetra-acetic acid (EDTA, Sigma-Aldrich). The tubes were spun down at 1,500 rpm for 10 minutes at 4°C and supernatants were gently taken off, after which PBS supplemented with 1% FCS and 2.5 mM EDTA was added to the pellets and tubes were spun down at 50 g for 3 minutes at 4°C. To separate the immune cells from the hepatocytes, the supernatant, which contains immune cells, was gently removed. The immune cells were spun down for 10 minutes at 1,600 rpm at 4°C. The supernatant was discarded, and 3 mL sterile PBS supplemented with 0.15M NH_4Cl; 1mM $KHCO_3$; 0.1 mM Na_2EDTA was added for 2 minutes to lyse red blood cells, followed by the addition of 7 mL PBS supplemented with 1% FCS and 2.5 mM EDTA (Sigma-Aldrich). The tubes were spun down for 10 minutes at 1,600 rpm at 4°C. The supernatant was discarded, and the pellet was resuspended in 10 mL PBS supplemented with 0.5% bovine serum albumin (Fraction V, Roche) and 10 mM ETDA (Sigma-Aldrich) and spun down for 10 minutes at 1,200 rpm at 4°C. The supernatant was removed, and 35 µL CD45 MicroBeads (Miltenyi Biotec) were added and incubated for 15 minutes in the fridge. After incubation the left-over beads were washed off by adding 10 mL PBS supplemented with 0.5% bovine serum albumin (Fraction V, Roche) and 10 mM ETDA and spun down for 10 minutes at 1,600 rpm at 4°C. The pellets were resuspended in 5 mL PBS supplemented with 0.5% BSA (Fraction V, Roche) and 10 mM ETDA and run through a pre-wetted LS magnetic column according to protocol (Miltenyi Biotec). The columns were washed with RPMI 1640 glutamax, 5% FCS, 0.1 % β-mercaptoethanol, 100U/mL penicillin, and 100 µg/mL streptomycin (culture medium) to collect the CD45$^+$ cells. The tubes were spun down for 10 minutes at 1,600 rpm at 4°C, supernatants were taken off and resuspended in 5 mL washing medium, and viable cells were counted using trypan blue and a Bürker counting chamber.

To process lungs, the lungs were chopped into small pieces using a scalpel and transferred to a 15-mL tube. To digest the tissue 5 mL RPMI 1640 glutamax supplemented with 1 mg/mL Collagenase IV (Sigma-Aldrich), 2 µL/mL DNase (Sigma-Aldrich), and 2 µL/mL of 1M $CaCL_2$ (Sigma-Aldrich) and incubated for 30 minutes at 37°C. After incubation, 10 mL cold RPMI 1640 glutamax with 5% FCS was added and poured through a 100-micron filter (BD). A 1 mL syringe was used to mash the digested tissue and washed with 20 mL cold RPMI 1640 glutamax with 5% FCS. The tubes were spun down for 10 minutes at 1,600 rpm at 4°C, and 2 mL sterile PBS supplemented with 0.15M NH_4Cl; 1mM $KHCO_3$; 0.1 mM Na_2EDTA was added for 2 minutes to lyse the red blood cells. After 2 minutes 8 mL of washing medium was added, and tubes were spun down for 10 minutes at 1,600 rpm at 4°C. Pellets were resuspended in 5 mL of washing medium, and viable cells were counted using trypan blue and a Bürker counting chamber.

Cell stimulation and analysis

200,000 cells per well were added. For specific restimulation, live *Plasmodium berghei* LA-GAP PbΔ*mei2* SPZ in a concentration of 25,000/mL (5,000 per 200,000 cells) in culture medium were added to each well and spun down for 4 minutes at 1,200 rpm at 4°C. For the aspecific restimulation, 0.1 µg/mL Phorbol 12-myristate 13-acetate (PMA) + 1 µg/mL iononomycin (Iono) (Sigma-Aldrich) in culture medium was added. To measure intracellular cytokine expression, 10 µg/mL Brefeldin A (Sigma-Aldrich) was directly added. All plates for flow-cytometry were incubated for 4 hours at 37°C with 5% CO_2.

After 4 hours (flow cytometry measurement), the cells were transferred into a V-bottom plate and washed with cold PBS. Cells were stained with live/dead marker Zombie NIR (Thermo Fisher), fixed with eBioscience FOXP3/Transcription Factor Fixation/Permeabilization kit, and stained with different markers for 3 different panels: (1) Myeloid panel (Table 1), (2) T-cell panel (Table 2), or (3) Advanced T-cell panel (Table 3, implemented halfway through the experiments). To all panels, Fc-block (BD bioscience), True-Stain Monocyte Blocker (BioLegend), and Brilliant Violet buffer (Thermo Fisher) was added. The cells were measured by flow cytometry using Aurora 5 laser (Cytek Bioscience B.V., Amsterdam) and analyzed using Spectroflow (Cytek Bioscience B.V.), Flowjo version 10.8 (FlowJo LLC), and R-studio version 1.4.1717. For gating strategy see Supplementary Figure 1.

Table 1. Myeloid Panel

Target	Antibody clone	Fluorochrome
MHCII	2G9	BUV395
PDL1	B7-H1	BUV737
CD11c	N418	BV421
Siglec F	E50-2440	BV480
CD40	3-23	BV510
CCR7	4B12	BV605
XCR1	ZET	BV650
F4/80	T45-2342	BV711
CD45	30-f11	BV785
CD70	FR70	FITC
Ly6C	HK1.4	PerCP-Cy5.5
CD80	16-10A1	PE
CD64	X54-5/7.1	PE-Dazzle
B220	RA3-6B2	PE-Cy5
CD11b	M1/70	PE-Cy7
CD206	C068C2	APC
TIM4	F31-5G3	AF647
CD86	GL1	AF700
NK1.1	PK135	APC-Cy7

Table 2. T-cell Panel

Target	Antibody clone	Fluorochrome
CD3	17A2	BUV661
CD45	30-F11	BUV805
CXCR3	CXCR3-173	Super Bright 436
Ki67	SolA15	eFluor 506
γδ T-cells	GL3	BV605
CD4	GK1.5	BV650
PDL1	10F.9G2	BV711
PD1	29f.1A12	BV785
Perforin	eBio0mak	FITC
CD44	1M7	AF532
CD8	53-6.7	PerCP
Granzyme A	GrA-368.5	PerCP-ef710
CD137	4-1BB	PE

CD69	H1.2F3	PE-cf594
IFNγ	XMG1.2	PE-Cy5
KLRG1	2F1	PE-Cy5.5
TNFα	MPG-XT22	PE-Cy7
FOXP3	FjK-16s	APC
Granzyme B	NGZB	efluor 660
CD25	PC61.5	AF700

Table 3. Advanced T-cell Panel

Target	Antibody clone	Fluorochrome
MHCII	2G9	BUV395
CD25	PC 61.5	BUV563
CD3	17A2	BUV661
CD62L	Mel-14	BUV737
CD45	30-f11	BUV805
CXCR3	CXCR3-173	Super Bright 436
γδ T-cells	GL3	BV605
CD4	GK1.5	BV650
CD11c	N418	BV711
PD1	29f.1A12	BV785
CD40L	SA047C3	FITC
CD44	IM7	AF532
CD8	53-6.7	PerCP
CD64	X54-5/7.1	PerCP-efluor 710
CD69	H1.2F3	PE-cf594
IFNγ	XMG1.2	PE-Cy5
KLRG1	2F1	PE-Cy5.5
TNFα	MPG-XT22	PE-Cy7
CD86	GL1	AF700
NK1.1	PK135	APC-Cy7

Statistical Analysis

Data were analyzed using Spectroflow (Cytek Bioscience B.V.), FlowJo version 10.8 (FlowJo LLC), R studio version 4.3.1, and Adobe illustrator 2023. Sample size estimation was performed with a power analysis using an alpha of 0.05 and a power of 90%. Statistical analyses were performed using one-way ANOVA with multiple comparisons with R studio version 4.3.1. Significance was defined as a p-value of less than 0.05. Data subjected to parametric statistical analyses had its normality confirmed beforehand.

Results

Distribution of Immune Cells in Liver and Lungs

To evaluate the potency of LA-GAP whole SPZ immunization, we analyzed the load of liver-stage parasites by bioluminescence. We confirmed that parasite liver loads were negative after the second immunization, suggesting full protection (Supplementary Figure 2). First, we investigated the overall kinetics of immune cell distribution in the liver and lungs 2 and 7 days after the last immunization. At the early timepoint we specifically looked at the innate cell compartments and found no differences in total number of myeloid cells (monocytes, dendritic cells, macrophages, neutrophils, and Kupffer cells in the liver) or B-cells in both liver and lungs after SPZ immunization compared with salivary gland extract (SGE, data not shown).

In the liver, we observed an early (2-day) increase of CD3$^+$ T cells (*P*=0.003, Figure 2A, C); whereas, in the lungs, we observed an early (2-day) and late (7-day) increase of CD3$^+$ T-cells after immunization of SPZs compared to SGE (*P*=0.003, Figure 2C). We subsequently gated the CD3$^+$ T-cell population on expression of CD4 and CD8 and found the T-cell increase was mainly attributed to an increased percentage of CD8$^+$ T cells (*P*<0.0001, *P*<0.0001, SPZ vs SGE for liver and lungs) with a reciprocal decrease in CD4$^+$ T cells (*P*<0.0001, *P*<0.0001, SPZ vs SGE for liver and lungs, respectively, Figure 2B). Interestingly, after immunization with dead SPZs we observed similar trends of immune cell recruitment, although the magnitude of CD8$^+$ T-cell recruitment seems to be lower in both organs as compared to live SPZ immunization (Figure 2B).

The dynamics of the CD3$^+$ T cells showed an overall important increase from day 2 to day 7 after immunization (mean increase 4.5%) in the lungs, whereas the reciprocal was true in the liver with overall CD3$^+$ cells decreased slightly over time (Figure 2C). Also, the total number of CD4$^-$ CD8$^-$ (double negative, DN) T cells (*P* =0.0003, Figure 2B) and Trm CD8$^+$ T cells (CD44^{hi} CD62L$^-$ CD69$^+$) (*P* =0.04, Figure 2E) increased from day 2 to 7 days after immunization in the lungs but not in the livers. Similarly, γδ T cells in the lungs showed a large increase of 2.5% over time but remained stable in the liver (Figure 2C), indicating that the total number of both CD3$^+$ and γδ T cells expands over time in the lungs but not in the liver. Moreover, we observed a significant increase in total number of natural killer (NK) cells (*P* =0.0009, Figure 2A) 2 days after immunization with SPZs in the lungs but not the livers. The early increased percentage of NK cells in the lungs was of a short duration as they decreased already at day 7 (mean 12.4% to 6.2% over time, Figure 2C). Finally, we found over time a trend for increased CD8$^+$ T-cell percentage in both organs (Figure 2D).

Within the $CD8^+$ T-cell population, mainly Tem $CD8^+$ T cells ($CD44^{hi}$ $CD62L^-$ $CD69^-$) were increased (*P* <0.0001, *P* <0.0001 SPZ vs SGE for liver and lungs, respectively, Figure 2E). The number of Trm $CD8^+$ T cells ($CD44^{hi}$ $CD62L^-$ $CD69^+$) was significantly increased in the lungs only (*P* =0.04, Figure 2E). Overall the DN T cells showed a complex dynamic, with a stable increase in the lungs only (Figure 2D). Expression of CD44 and CD25 on DN T cells significantly decreased in the liver (*P* =0.0001) and showed a decreased trend of expression in the lungs after SPZ immunization. This resulted in an increase of DN4 cells (*P* <0.0001, *P* =0.0003 SPZ vs SGE for liver and lungs, respectively), which are known for differentiation into γδ T cells, $CD4^+$ or $CD8^+$ T cells (Figure 2F).

Collectively, changes in immune cell distribution after SPZ immunization, notably in the NK cell population, the overall $CD3^+$ T-cell population, γδ T-cell population, and $CD8^+$ T-cell population, in particular the Trm $CD8^+$ T-cells, were more pronounced in the lungs than the liver. In general, the lungs thus seem to recruite a more diverse pallet of different cell types, and for a longer duration after SPZ immunization as compared with the liver.

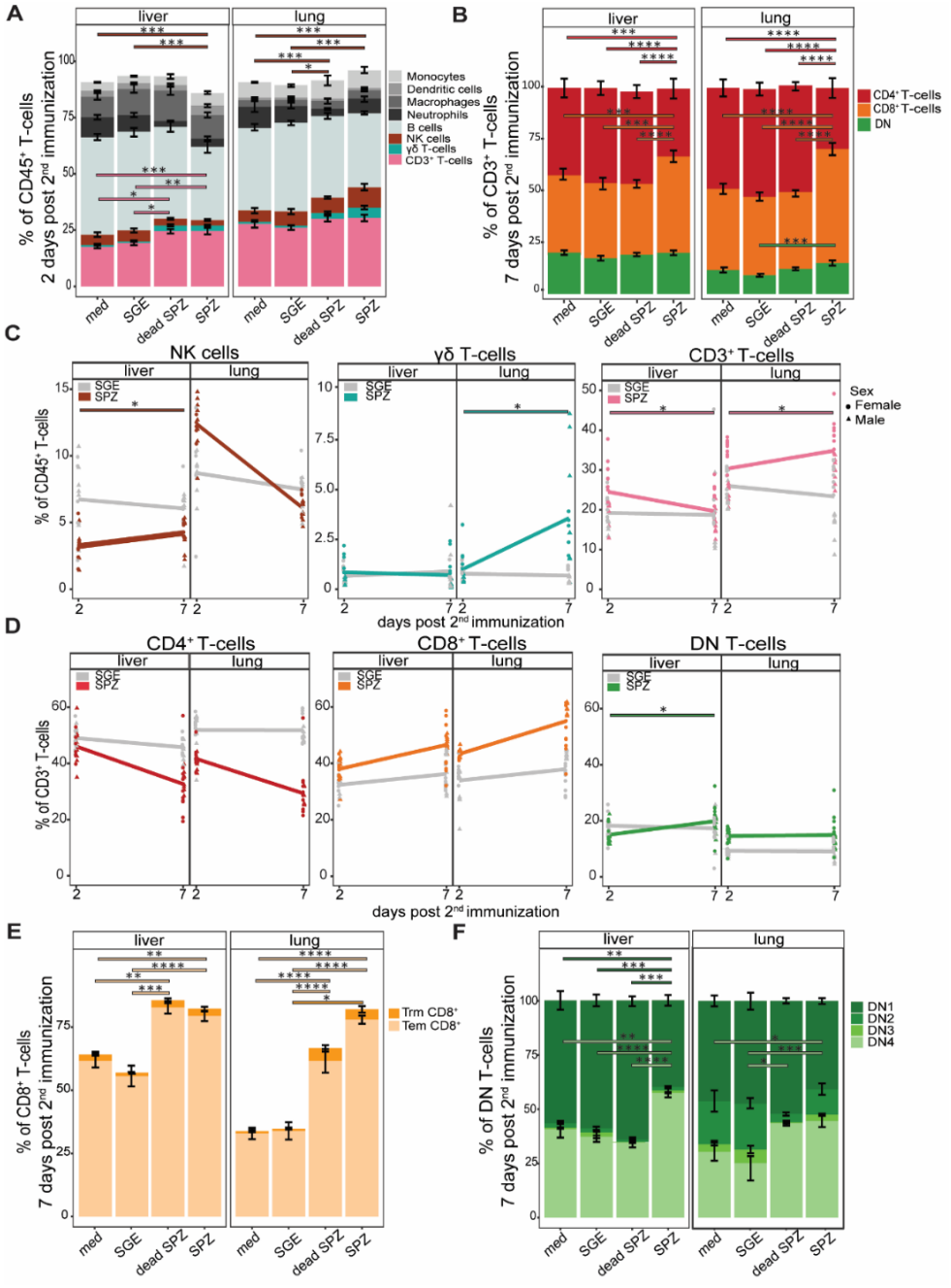

Figure 2. Distribution of different cell types. **(A)** Percentage (gated out of CD45⁺ live cells) of monocytes (light grey), dendritic cells (grey), macrophages (dark grey), neutrophils (black), B-cells (blue grey), NK cells (brown), γδ T cells (turquoise), CD3⁺ T cells (pink), in liver

and lungs after immunization with medium (med), salivary gland extract (SGE), dead sprozoites (SPZ), or live SPZ, 2 days post second immunization. (B) Distribution of $CD4^+$ T cells (red), $CD8^+$ T cells (orange), and DN T-cells (green), in liver and lungs after immunization with medium, SGE, dead SPZ, or SPZ, 7 days post second immunization. (C) Changes in distribution of NK cells, γδ T cells, or $CD3^+$ T cells over time between days 2 to 7 post second immunization. SGE-injected mice in grey, SPZ-injected mice in brown for NK cells, turquoise for γδ T cells, or pink for $CD3^+$ T cells. (D) Changes in distribution of $CD4^+$ T cells, $CD8^+$ T cells, or DN T cells over time between days 2 to 7 post second immunization. SGE-injected mice in grey, SPZ-injected mice in red for $CD4^+$ T cells, orange for $CD8^+$ T cells, or green for DN T cells. (E) Number of Tem (light orange) and Trm (orange) $CD8^+$ T cells in liver and lungs after immunization with medium, SGE, dead SPZ, or SPZ, 7 days post second immunization. (F) Number of DN1, DN2, DN3, and DN4 cells in different shades of green in liver and lungs after immunization with medium, SGE, dead SPZ, or SPZ, 7 days post second immunization. Med n=14, SGE n=18, dead SPZ n=10, SPZ n=18, divided over 2 (dead SPZ) or 3 (med, SGE, SPZ) experiments. Statistical significance between groups was assessed by one-way ANOVA with multiple comparisons. *P<0.05, **P <0.005, ***P<0.0005, and ****P<0.0001.

Cellular Activation

Having shown dynamic changes in mainly T cells in both organs, we next investigated the activation status of these cells at 7 days post second immunization following *ex vivo* restimulation with SPZs. An optimized t-Ditributed Stochastic Neighbor Embedding (opt-SNE) analysis based on different T-cell markers revealed activation of 2 cell clusters after SPZ immunization, which were not activated after SGE immunization. We found that these clusters consisted of $CD8^+$ T cells and DN T cells (Figure 3A+B). Activation of the $CD8^+$ T cells was characterized by an increase in CD11c (P<0.0001, P<0.0001), Ki67 (P<0.0001, P<0.0001), and KLRG1 (P<0.0001, P<0.0001) in both liver and lungs after SPZ immunization compared with SGE (Figure 3C, Supplementary Figure 3A+B). Impressively, we observed that almost half of the $CD8^+$ T cells express CD11c and/or Ki67 in both liver and lungs after SPZ immunization. In the DN T cells, we observed a similar pattern of activation markers for both organs after SPZ immunization, with increases in CD11c (P<0.0001, P<0.0001), Ki67 (P<0.0001, P<0.0001), and KLRG1 (P<0.0001, P<0.0001) (Figure 3D, Supplementary Figure 3C+D). Over time we observed in both organs an increased percentage of $Ki67^+$ $CD8^+$ T cells and $Ki67^+$ DN T cells, while the percentage of $KLRG1^+$ $CD8^+$ T cells, $KLRG1^+$ DN T cells, $CD11c^+$ $CD8^+$ T cells, and $CD11c^+$ DN T cells stayed stable (Supplementary Figure 3E+F). We found an increase in $CD137^+$ DN^+ T cells for the liver only (P=0.02) and not for the lungs. On the contrary, the lungs showed an increased expression of proliferation marker Ki67 and a significant increase in proliferation marker KLRG1 on γδ T cells (P= 0.0004, Supplementary Figure

4A). Interestingly, we hardly observed any activation of immune cells after immunization with dead SPZs in both liver and lungs (Figure 3C+D, Supplementary Figure 3A, B, C, D, Supplementary Figure 5A).

As for the innate compartments 2 days post second immunization, both organs showed an increased trend in expression of KLRG1 on NK cells after SPZ immunization (Supplementary Figure 4B). In the liver, macrophages showed an upregulation of both activation and regulatory markers (CD80 *P*=0.0006 and PDL1 *P*=0.007, Supplementary Figure 5B), whereas in the lungs, no activation of macrophages was found but only increases in the regulatory marker PDL-1 (Supplementary Figure 5A). These regulatory macrophages were further phenotyped as interstitial macrophages (Supplementary Figure 6C). In the liver we found an increased trend in expression on monocytes (CD80 and CD86, Supplementary Figure 6A), which was absent in the lungs.
In conclusion, activated cells were mainly found within the CD8+ T cell and DN T cell compartments and after immunization with live SPZs. Here, there were only slight phenotypic differences between lung and liver. However, the phenotype of macrophages and monocytes was different between liver and lungs, with activation markers on both cells only found in the liver.

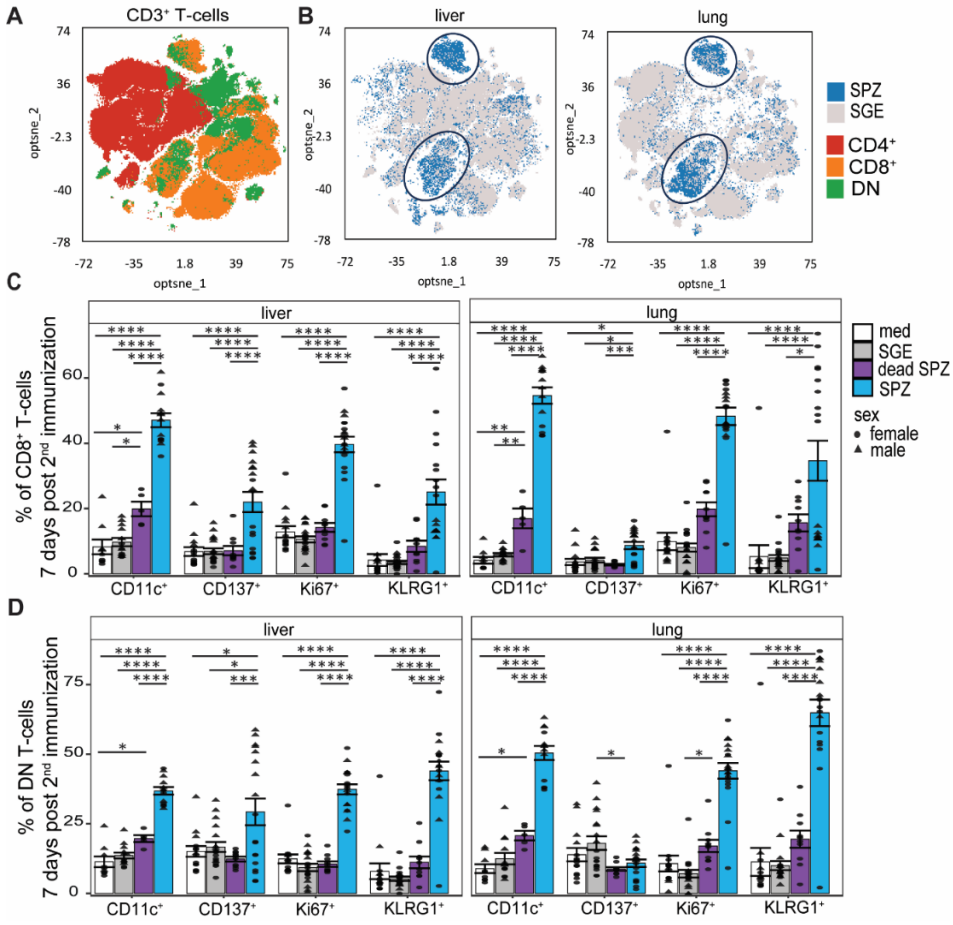

Figure 3. Cellular activation. (A) Optimized t-Ditributed Stochastic Neighbor Embedding with CD8⁺ T cells in orange, CD4⁺ T-cells in red, and DN T-cells in green. (B) Optimized t-Ditributed Stochastic Neighbor Embedding T-cell overlay of SPZ-injected (blue) or SGE_injected (grey) mice. (C) CD11c⁺, CD137⁺, Ki67⁺, and KLRG1⁺ CD8⁺ T cells after immunization with medium (white), SGE (grey), dead SPZ (purple), or SPZ (blue). (D) CD11c⁺, CD137⁺, Ki67⁺, and KLRG1⁺ DN T cells after immunization with medium (white), SGE (grey), dead SPZ (purple), or SPZ (blue) 7 days post second immunization. Male mice showed by triangle and female mice showed by circle symbol, restimulated with SPZs. CD137, Ki67, and KLRG1: med n=14, SGE n=18, dead SPZ n=10, SPZ n=18, divided over 2 (dead SPZ) or 3 (med, SGE, SPZ) experiments. CD11c: med n=9, SGE n=13, dead SPZ n=9, SPZ n=13, divided over 2 experiments. Statistical significance between groups was assessed by one-way ANOVA with multiple comparisons. *P<0.05, **P<0.005, ***P<0.0005, and ****P<0.0001.

T-cell Killing Pathway

Having shown an increase in percentage of activated CD8+ T cells and DN T cells in the liver and lungs, we next investigated the functionality of these cells by measuring Granzyme A, Granzyme B, and perforin expression 7 days after the last immunization after *ex vivo* restimulation with SPZ. Interestingly, we observed that CD8+ T cells in both organs displayed an increased expression of Granzyme A but not Granzyme B or perforin when injected with SPZs compared with SGE (P=0.0002, P<0.0001, Figure 4A+B+C+D). Again, this observation was specific for live SPZ immunization only, as Granzyme A expression was not increased after dead SPZ immunization (Figure 4B+D).

When looking into organ-specific differences, we found the magnitude of expression of Granzyme A was roughly 4-fold higher in lungs as compared to liver. For DN T cells, on the contrary, we observed a significant increase of Granzyme A expression in the liver (P=0.015) and a lower trend of increased expression in the lungs after SPZ immunization compared with SGE immunization (Figure 4C+D). Interestingly, here we observed some sex-specific differences in immune functionality where, for both the CD8+ T cells and DN T cells in the lungs, a higher expression of Granzyme A appeared in male mice than in female mice (Figure 4B+D).

Collectively, functionality of CD8+ T cells and DN T cells seems to be mediated by Granzyme A after SPZ immunization in the lungs.

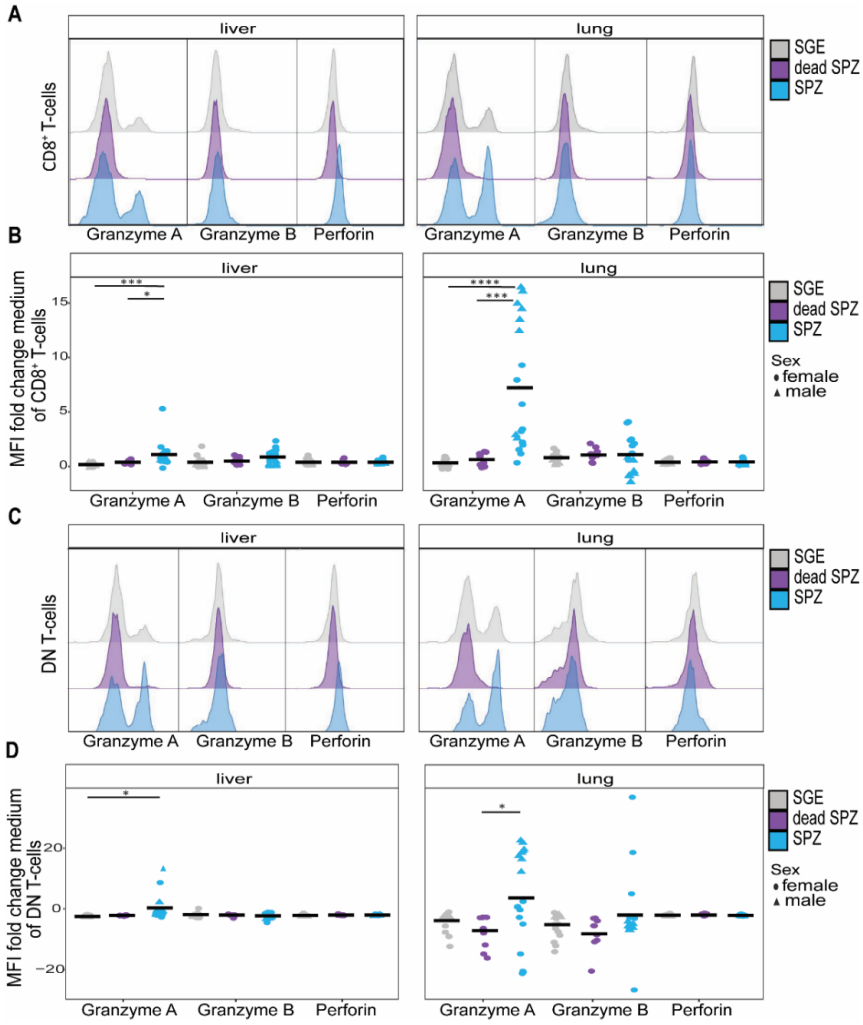

Figure 4. T-cell functionality. (A) Histogram of Granzyme A, Granzyme B, or perforin expression on $CD8^+$ T cells after SGE (grey), dead SPZ (purple), or SPZ (blue) immunization. (B) Mean expression of Granzyme A, Granzyme B, or perforin on $CD8^+$ T cells after SGE (grey), dead SPZ (purple), or SPZ (blue) immunization, fold change to medium. (C) Histogram of Granzyme A, Granzyme B, or perforin expression on DN T cells after SGE (grey), dead SPZ (purple), or SPZ (blue) immunization. (D) Mean expression of Granzyme A, Granzyme B, or perforin on DN T cells after SGE (grey), dead SPZ (purple), or SPZ (blue) immunization, fold change to medium. All data from 7 days post second immunization. Male mice showed by triangle and female mice showed by circle symbol, cells restimulated with SPZ. Med n=14, SGE n=18, dead SPZ n=10, SPZ n=18, divided over 2 (dead SPZ) or 3 (med, SGE, SPZ) experiments. Statistical significance between groups was assessed by one-way ANOVA with multiple comparisons. *P<0.05, **P<0.005, ***P<0.0005, and ****P<0.0001.

T-cell Cytokine Expression

Finally, we investigated the cytokine expression patterns of these CD8⁺ T cells and DN T cells in the liver and lungs 7 days post second immunization and after *ex vivo* restimulation with SPZs by measuring intracellular TNF and IFNγ by flow cytometry. Here, we observed a significant increase of TNF expression in CD8⁺ T cells (P=0.0002) and DN T cells (P<0.0001) in the liver and CD8⁺ T cells (P<0.0001) and DN T cells (P<0.0001) in the lungs (Figure 5A). This was specific to live SPZ immunization, as the increased expression of TNF after dead SPZ immunization was modest and significantly lower compared with live SPZ (liver; P=0.001, lung; P<0.0001). Increases were more pronounced in the lungs as compared with the liver (TNF⁺ CD8⁺ T cells P=0.007 and TNF⁺ DN T-cells P=0.04, Figure 5A). These differences start already at the early 2-day timepoint at which the lungs show a 10.2 % increase in TNF⁺ CD8⁺ T cells and the liver shows a more modest increase of 2.6 % (Figure 5B, Supplementary Figure 5A). Moreover, γδ T cells showed an increased expression of TNF only in the lungs after SPZ immunization compared with SGE (P=0.007) but not in the liver (Supplementary Figure 5E).

For IFNγ, we observed a different pattern of expression, as IFNγ⁺ CD8⁺ T cells increase only in the liver (2.7 % increase SPZ vs SGE) and not in the lungs (Figure 5C). This increase resulted in a significant difference in IFNγ⁺ CD8⁺ T cells between the liver and lungs (P=0.0007, Figure 5C). However, *ex vivo* restimulation with PMA/Iono instead of SPZs, which says something about the functionality of the cells instead of specificity, showed an increase of IFNγ⁺ CD8⁺ T cells (P<0.0001) and IFNγ⁺ DN T cells (P<0.0001) in the lung, which was 17% (CD8⁺ T cells) and 23% (DN T cells) higher compared with the liver (Figure 5E+F).

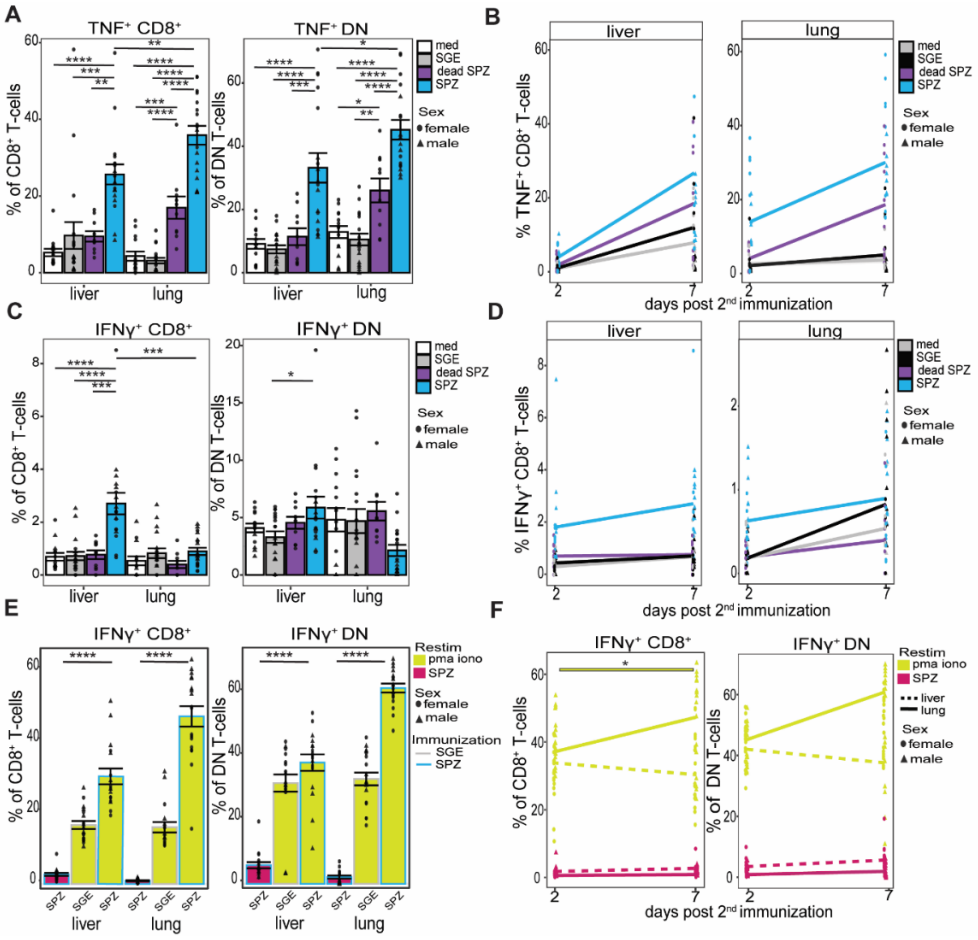

Figure 5. T-cell cytokine functionaility. (A) Percentage of TNF⁺ CD8⁺ T cells and TNF⁺ DN T cells after medium (white), SGE (grey), dead SPZ (purple), or SPZ (blue) 7 days post second immunization after SPZ restimulation. (B) Percentage of TNF⁺ CD8⁺ T cells over time, from 2 to 7 days post second immunization after SPZ restimulation. (C) Percentage of IFNγ⁺ CD8⁺ T cells and IFNγ⁺ DN T cells after medium (white), SGE (grey), dead SPZ (purple), or SPZ (blue) 7 days post second immunization after SPZ restimulation. (D) Percentage of IFNγ⁺ CD8⁺ T cells over time, from 2 to 7 days post second immunization after SPZ restimulation. (E) Percentage IFNγ⁺ CD8⁺ T cells and IFNγ⁺ DN T cells of SPZ or SGE injected mice after SPZ (pink) or PMA/Iono (yellow) restimulation, 7 days post second immunization. (F) Percentage IFNγ⁺ CD8⁺ T cells and IFNγ⁺ DN T cells over time from 2 to 7 days post second immunization, following SPZ (pink) or PMA/Iono (yellow) restimulation. Interrupted line for liver and smooth line for lungs. Med n=14, SGE n=18, dead SPZ n=10, SPZ n=18, divided over 2 (dead SPZ) or 3 (med, SGE, SPZ) experiments. Male mice showed by triangle and female mice showed by circle symbol. Statistical significance between groups was assessed by one-way

ANOVA with multiple comparisons. *P<0.05, **P<0.005, ***P=<0.0005 and ****: P=<0.0001.

Also CD4⁺ T-cells expressed IFNγ to a higher extent in the liver as compared with the lungs after SPZ immunization with SPZ restimulation. Similarly to the CD8⁺ T-cells, these cells could be readily activated with a 2-fold increase in IFNγ expression CD4⁺ T-cells and a 7-fold increase in γδ T-cells in the lungs after *ex vivo* restimulation with PMA/Iono compared with SPZ, which was not observed in the liver (Supplementary Figure 5D+F).

Overall, we demonstrated that mainly CD8⁺ T-cells and DN T cells in the lungs are increased in number and activation after SPZ immunization. These lung T cells express Granzyme A and TNF after SPZ restimulation but less IFNγ. After aspecific PMA/Iono restimulation, however, they also readily produce IFNγ.

Discussion

Here, we compared the immune response to LA-GAP immunization in the liver and lungs in a rodent malaria model. Surprisingly, we found that responses in the lungs were overall more pronounced than in liver, particularly in the CD8⁺, DN, and γδ T-cell compartments, and lung cells displayed an increased expression of pro-inflammatory activation markers and cytokines. Most immune changes were specific to immunization with live SPZ and could not be found after immunization with dead SPZ. These results thus suggest that the lungs may be a key organ in mediating protection after LA-GAP immunization.

SPZ make use of the host circulatory system to travel to the liver. Inherent to the anatomy of the circulatory system, SPZ must pass the lungs before being able to reach the target organ. Because of the narrow diameter of lung capillaries (3-5 µm in mice [22]), SPZ (10-15 µm in length and 1.5 µm in width [23]) must actively navigate to pass this organ. This short interaction of the SPZ with its surrounding tissue provides the host with an opportunity to harness innate cells such as macrophages to capture SPZ and activate the adaptive immune system [24-26]. However, the overall impact of the interaction and the ensuing immune response has not been studied before.

For other hematogenous parasites like *Schistosoma* and *Trypanosoma* and parasites that utilize the bloodstream such as *Toxoplasma* and *Leishmania,* it has been known that they can activate CD8⁺ T cells and kill parasite infected cells in the lungs [27-30]. Moreover, from pulmonary viral and bacterial infections, it is known that lung CD8⁺ T cells can upregulate multiple activation markers such as IFNγ and TNF in different

murine models and that these activated cells are critical for mediating pathogen clearance [31, 32]. Even though the route of entering the lungs might differ per pathogen, similarities in the expression profile of IFNγ and TNF on $CD8^+$ T cells makes us hypothesize that the immune cells in the lungs play a comparable role in mediating SPZ clearance after immunization of LA-GAP SPZ.
Also, for Plasmodium, $CD8^+$ T cells were shown to mediate critical protection in rodent and non-human primate studies. Using radiation-attenuated SPZ (RAS) immunization models, DCs in the spleen, liver, and liver-draining lymph nodes were shown to present antigens, likely via antigen cross-presentation, to $CD8^+$ T cells [33-35]. Depletion of $CD8^+$ T cells consequently abrogated the immunity induced by RAS immunization, proving they play a key role in mediating protection in the liver [36]. Moreover, liver Trm $CD8^+$ T cells were able to directly kill infected hepatocytes through secretion of perforin and Granzyme B [9, 19] likely with a complementary function of Granzyme A in early responses [37]. In the current study, we find a similar phenotype of $CD8^+$ T cells in the lungs, again supporting the hypothesis that these cells may also be able to mediate protection. The regulatory macrophage phenotype, which we found earlier in the lungs, has previously been described after SPZ uptake [38], leading us to believe that lung macrophages are able to take up SPZ and may play a role in T-cell priming after LA-GAP inoculation.

However, it remains unclear whether these $CD8^+$ T cells, once primed in the lungs, are capable of directly killing SPZs within the lungs, thus reducing the number of SPZs that reach the liver, or if they migrate to the liver to specifically target infected hepatocytes. However, judging by their phenotype, the Tem cells we identified in the lungs, unlike Trm, retain the ability to migrate to other organs. In addition, we observed a stark increase of $CD11c^+$ $CD8^+$ T cells, which co-express Ki67 and KLRG1, in the lungs. It has been proven that cells with the same phenotype in the liver can inhibit liver-stage parasite development *in vitro* [39]. This suggests that T cells may initially be primed in the lungs before migrating to the liver, where they could potentially eliminate infected hepatocytes. The impact of these findings on $CD8^+$-mediated killing of malaria-infected hepatocytes thus depends on their capability to recirculate.

Despite considerable differences between humans and rodents, we argue that our findings are nonetheless relevant to human LA-GAP programs. The pulmonary capillary diameters of mice (3-5 µm [22]) and humans (1-7.5 µm, mean 3.7 µm) are comparable [40], meaning that human immune cells can similarly encounter SPZs in the lungs. Moreover, we observed a comparable T-cell increase and phenotype of CD69 expressing

CD8+ Trm T cells in mice lungs and livers as has been described in human livers of ChAd63 MVA ME-TRAP vaccinated volunteers associated with a reduced risk of developing malaria [41]. In a recent human clinical trial with mosquito bite-administered LA-GAP, we showed high-level protection could be achieved with just a single immunisation [42]. How a potential future change in the route of administration from mosquito bite to direct venous inoculation, with higher numbers of LA-GAP passing the lung, may potentially affect downstream protection remains to be investigated.

In conclusion, we compared organ-specific immune responses in lungs and liver after LA-GAP immunization and found impressive activation of CD8+ and DN T cells, particularly in the lungs. These observations suggest a pivotal role for the lungs as a priming immune organ and warrant further investigation to further our understanding of the full potential of LA-GAP immunization as a powerful tool to combat malaria.

Acknowledgments

We would like to thank the flow cytometry facility of the LUMC.

References

1. Osoro CB, Ochodo E, Kwambai TK, Otieno JA, Were L, Sagam CK, Owino EJ, Kariuki S, Ter Kuile FO, Hill J. Policy uptake and implementation of the RTS,S/AS01 malaria vaccine in sub-Saharan African countries: status 2 years following the WHO recommendation. *BMJ Glob Health*. 2024;9(4). doi: 10.1136/bmjgh-2023-014719. PubMed PMID: 38688566; PMCID: PMC11085798.
2. Goh YS, McGuire D, Renia L. Vaccination With Sporozoites: Models and Correlates of Protection. *Front Immunol*. 2019;10:1227. doi: 10.3389/fimmu.2019.01227. PubMed PMID: 31231377; PMCID: PMC6560154.
3. Itsara LS, Zhou Y, Do J, Grieser AM, Vaughan AM, Ghosh AK. The Development of Whole Sporozoite Vaccines for Plasmodium falciparum Malaria. *Front Immunol*. 2018;9:2748. doi: 10.3389/fimmu.2018.02748. PubMed PMID: 30619241; PMCID: PMC6297750.
4. Hassert M, Arumugam S, Harty JT. Memory CD8+ T cell-mediated protection against liver-stage malaria. *Immunol Rev*. 2023;316(1):84-103. doi: 10.1111/imr.13202. PubMed PMID: 37014087; PMCID: PMC10524177.
5. Butler NS, Vaughan AM, Harty JT, Kappe SH. Whole parasite vaccination approaches for prevention of malaria infection. *Trends Immunol*. 2012;33(5):247-54. doi: 10.1016/j.it.2012.02.001. PubMed PMID: 22405559.
6. Franke-Fayard B, Marin-Mogollon C, Geurten FJA, Chevalley-Maurel S, Ramesar J, Kroeze H, Baalbergen E, Wessels E, Baron L, Soulard V, Martinson T, Aleshnick M, Huijs ATG, Subudhi AK, Miyazaki Y, Othman AS, Kolli SK, Lamers OAC, Roques M, Stanway RR, Murphy SC, Foquet L, Moita D, Mendes AM, Prudencio M, Dechering KJ, Heussler VT, Pain A, Wilder BK, Roestenberg M, Janse CJ. Creation and preclinical evaluation of genetically attenuated malaria parasites arresting growth late in the liver. *NPJ Vaccines*. 2022;7(1):139. doi: 10.1038/s41541-022-00558-x. PubMed PMID: 36333336; PMCID: PMC9636417.
7. Lamers OAC, Franke-Fayard BMD, Koopman JPR, Roozen GVT, Janse JJ, Chevalley-Maurel SC, Geurten FJA, de Bes-Roeleveld HM, Iliopoulou E, Colstrup E, Wessels E, van Gemert GJ, van de Vegte-Bolmer M, Graumans W, Stoter TR, Mordmuller BG, Houlder EL, Bousema T, Murugan R, McCall MBB, Janse CJ, Roestenberg M. Safety and Efficacy of Immunization with a Late-Liver-Stage Attenuated Malaria Parasite. *N Engl J Med*. 2024;391(20):1913-23. doi: 10.1056/NEJMoa2313892. PubMed PMID: 39565990.
8. Yadav N, Parthiban C, Billman ZP, Stone BC, Watson FN, Zhou K, Olsen TM, Cruz Talavera I, Seilie AM, Kalata AC, Matsubara J, Shears MJ, Reynolds RA, Murphy

SC. More time to kill: A longer liver stage increases T cell-mediated protection against pre-erythrocytic malaria. *iScience*. 2023;26(12):108489. doi: 10.1016/j.isci.2023.108489. PubMed PMID: 38162031; PMCID: PMC10755051.

9. Lefebvre MN, Harty JT. You Shall Not Pass: Memory CD8 T Cells in Liver-Stage Malaria. *Trends Parasitol*. 2020;36(2):147-57. doi: 10.1016/j.pt.2019.11.004. PubMed PMID: 31843536; PMCID: PMC6937381.
10. Lefebvre MN, Surette FA, Anthony SM, Vijay R, Jensen IJ, Pewe LL, Hancox LS, Van Braeckel-Budimir N, van de Wall S, Urban SL, Mix MR, Kurup SP, Badovinac VP, Butler NS, Harty JT. Expeditious recruitment of circulating memory CD8 T cells to the liver facilitates control of malaria. *Cell Rep*. 2021;37(5):109956. doi: 10.1016/j.celrep.2021.109956. PubMed PMID: 34731605; PMCID: PMC8628427.
11. Carvalho LH, Sano G, Hafalla JC, Morrot A, Curotto de Lafaille MA, Zavala F. IL-4-secreting CD4+ T cells are crucial to the development of CD8+ T-cell responses against malaria liver stages. *Nat Med*. 2002;8(2):166-70. doi: 10.1038/nm0202-166. PubMed PMID: 11821901.
12. Ribot JC, Neres R, Zuzarte-Luís V, Gomes AQ, Mancio-Silva L, Mensurado S, Pinto-Neves D, Santos MM, Carvalho T, Landry JJM, Rolo EA, Malik A, Silva DV, Mota MM, Silva-Santos B, Pamplona A. γδ-T cells promote IFN-γ-dependent pathogenesis upon liver-stage infection. *P Natl Acad Sci USA*. 2019;116(20):9979-88. doi: 10.1073/pnas.1814440116. PubMed PMID: WOS:000467804000049.
13. Radtke AJ, Tse SW, Zavala F. From the draining lymph node to the liver: the induction and effector mechanisms of malaria-specific CD8+ T cells. *Semin Immunopathol*. 2015;37(3):211-20. doi: 10.1007/s00281-015-0479-3. PubMed PMID: 25917387; PMCID: PMC5600878.
14. Chakravarty S, Cockburn IA, Kuk S, Overstreet MG, Sacci JB, Zavala F. CD8+ T lymphocytes protective against malaria liver stages are primed in skin-draining lymph nodes. *Nat Med*. 2007;13(9):1035-41. doi: 10.1038/nm1628. PubMed PMID: 17704784.
15. Obeid M, Franetich JF, Lorthiois A, Gego A, Grüner AC, Tefit M, Boucheix C, Snounou G, Mazier D. Skin-draining lymph node priming is sufficient to induce sterile immunity against pre-erythrocytic malaria. *Embo Mol Med*. 2013;5(2):250-63. doi: 10.1002/emmm.201201677. PubMed PMID: WOS:000314661800011.

16. Sinnis P, Zavala F. The skin: where malaria infection and the host immune response begin. *Semin Immunopathol*. 2012;34(6):787-92. doi: 10.1007/s00281-012-0345-5. PubMed PMID: 23053392; PMCID: PMC3934925.
17. Behboudi S, Moore A, Hill AV. Splenic dendritic cell subsets prime and boost CD8 T cells and are involved in the generation of effector CD8 T cells. *Cell Immunol*. 2004;228(1):15-9. doi: 10.1016/j.cellimm.2004.03.010. PubMed PMID: 15203315.
18. Cockburn IA, Seder RA. Malaria prevention: from immunological concepts to effective vaccines and protective antibodies. *Nat Immunol*. 2018;19(11):1199-211. doi: 10.1038/s41590-018-0228-6. PubMed PMID: 30333613.
19. Fernandez-Ruiz D, Ng WY, Holz LE, Ma JZ, Zaid A, Wong YC, Lau LS, Mollard V, Cozijnsen A, Collins N, Li J, Davey GM, Kato Y, Devi S, Skandari R, Pauley M, Manton JH, Godfrey DI, Braun A, Tay SS, Tan PS, Bowen DG, Koch-Nolte F, Rissiek B, Carbone FR, Crabb BS, Lahoud M, Cockburn IA, Mueller SN, Bertolino P, McFadden GI, Caminschi I, Heath WR. Liver-Resident Memory CD8(+) T Cells Form a Front-Line Defense against Malaria Liver-Stage Infection. *Immunity*. 2019;51(4):780. doi: 10.1016/j.immuni.2019.09.019. PubMed PMID: 31618655.
20. Fougere A, Jackson AP, Bechtsi DP, Braks JA, Annoura T, Fonager J, Spaccapelo R, Ramesar J, Chevalley-Maurel S, Klop O, van der Laan AM, Tanke HJ, Kocken CH, Pasini EM, Khan SM, Bohme U, van Ooij C, Otto TD, Janse CJ, Franke-Fayard B. Correction: Variant Exported Blood-Stage Proteins Encoded by Plasmodium Multigene Families Are Expressed in Liver Stages Where They Are Exported into the Parasitophorous Vacuole. *PLoS Pathog*. 2017;13(1):e1006128. doi: 10.1371/journal.ppat.1006128. PubMed PMID: 28095481; PMCID: PMC5240906.
21. Annoura T, Chevalley S, Janse CJ, Franke-Fayard B, Khan SM. Quantitative analysis of Plasmodium berghei liver stages by bioluminescence imaging. *Methods Mol Biol*. 2013;923:429-43. doi: 10.1007/978-1-62703-026-7_30. PubMed PMID: 22990796.
22. Steinman J, Koletar MM, Stefanovic B, Sled JG. 3D morphological analysis of the mouse cerebral vasculature: Comparison of in vivo and ex vivo methods. *PLoS One*. 2017;12(10):e0186676. doi: 10.1371/journal.pone.0186676. PubMed PMID: 29053753; PMCID: PMC5650181.

23. Sinden RE, Butcher GA, Beetsma AL. Maintenance of the Plasmodium berghei life cycle. *Methods Mol Med*. 2002;72:25-40. doi: 10.1385/1-59259-271-6:25. PubMed PMID: 12125122.
24. Chua CLL, Ng IMJ, Yap BJM, Teo A. Factors influencing phagocytosis of malaria parasites: the story so far. *Malar J*. 2021;20(1):319. doi: 10.1186/s12936-021-03849-1. PubMed PMID: 34271941; PMCID: PMC8284020.
25. Corradin G, Levitskaya J. Priming of CD8(+) T Cell Responses to Liver Stage Malaria Parasite Antigens. *Front Immunol*. 2014;5:527. doi: 10.3389/fimmu.2014.00527. PubMed PMID: 25414698; PMCID: PMC4220712.
26. Kurup SP, Butler NS, Harty JT. T cell-mediated immunity to malaria. *Nat Rev Immunol*. 2019;19(7):457-71. doi: 10.1038/s41577-019-0158-z. PubMed PMID: 30940932; PMCID: PMC6599480.
27. Khan IA, Hwang S, Moretto M. Toxoplasma gondii: CD8 T Cells Cry for CD4 Help. *Front Cell Infect Microbiol*. 2019;9:136. doi: 10.3389/fcimb.2019.00136. PubMed PMID: 31119107; PMCID: PMC6504686.
28. Ali Z, Kosanovic D, Kolosionek E, Schermuly RT, Graham BB, Mathie A, Butrous G. Enhanced inflammatory cell profiles in schistosomiasis-induced pulmonary vascular remodeling. *Pulm Circ*. 2017;7(1):244-52. doi: 10.1086/690687. PubMed PMID: 28680583; PMCID: PMC5448541.
29. Mabille D, Dirkx L, Thys S, Vermeersch M, Montenye D, Govaerts M, Hendrickx S, Takac P, Van Weyenbergh J, Pintelon I, Delputte P, Maes L, Perez-Morga D, Timmermans JP, Caljon G. Impact of pulmonary African trypanosomes on the immunology and function of the lung. *Nat Commun*. 2022;13(1):7083. doi: 10.1038/s41467-022-34757-w. PubMed PMID: 36400767; PMCID: PMC9674601.
30. Stager S, Rafati S. CD8(+) T cells in leishmania infections: friends or foes? *Front Immunol*. 2012;3:5. doi: 10.3389/fimmu.2012.00005. PubMed PMID: 22566891; PMCID: PMC3342007.
31. Ostler T, Davidson W, Ehl S. Virus clearance and immunopathology by CD8(+) T cells during infection with respiratory syncytial virus are mediated by IFN-gamma. *Eur J Immunol*. 2002;32(8):2117-23. doi: 10.1002/1521-4141(200208)32:8<2117::AID-IMMU2117>3.0.CO;2-C. PubMed PMID: 12209623.
32. Lucas R, Hadizamani Y, Enkhbaatar P, Csanyi G, Caldwell RW, Hundsberger H, Sridhar S, Lever AA, Hudel M, Ash D, Ushio-Fukai M, Fukai T, Chakraborty T, Verin A, Eaton DC, Romero M, Hamacher J. Dichotomous Role of Tumor Necrosis Factor in Pulmonary Barrier Function and Alveolar Fluid Clearance.

Front Physiol. 2021;12:793251. doi: 10.3389/fphys.2021.793251. PubMed PMID: 35264975; PMCID: PMC8899333.

33. Jobe O, Donofrio G, Sun G, Liepinsh D, Schwenk R, Krzych U. Immunization with radiation-attenuated Plasmodium berghei sporozoites induces liver cCD8alpha+DC that activate CD8+T cells against liver-stage malaria. *PLoS One*. 2009;4(4):e5075. doi: 10.1371/journal.pone.0005075. PubMed PMID: 19347042; PMCID: PMC2661143.
34. Schmidt NW, Butler NS, Badovinac VP, Harty JT. Extreme CD8 T cell requirements for anti-malarial liver-stage immunity following immunization with radiation attenuated sporozoites. *PLoS Pathog*. 2010;6(7):e1000998. doi: 10.1371/journal.ppat.1000998. PubMed PMID: 20657824; PMCID: PMC2904779.
35. Parmar R, Patel H, Yadav N, Parikh R, Patel K, Mohankrishnan A, Bhurani V, Joshi U, Dalai SK. Infectious Sporozoites of Plasmodium berghei Effectively Activate Liver CD8alpha(+) Dendritic Cells. *Front Immunol*. 2018;9:192. doi: 10.3389/fimmu.2018.00192. PubMed PMID: 29472929; PMCID: PMC5809440.
36. Van Braeckel-Budimir N, Harty JT. CD8 T-cell-mediated protection against liver-stage malaria: lessons from a mouse model. *Front Microbiol*. 2014;5:272. doi: 10.3389/fmicb.2014.00272. PubMed PMID: 24936199; PMCID: PMC4047659.
37. Hermsen CC, Konijnenberg Y, Mulder L, Loe C, van Deuren M, van der Meer JW, van Mierlo GJ, Eling WM, Hack CE, Sauerwein RW. Circulating concentrations of soluble granzyme A and B increase during natural and experimental Plasmodium falciparum infections. *Clin Exp Immunol*. 2003;132(3):467-72. doi: 10.1046/j.1365-2249.2003.02160.x. PubMed PMID: 12780694; PMCID: PMC1808730.
38. Winkel BMF, Pelgrom LR, van Schuijlenburg R, Baalbergen E, Ganesh MS, Gerritsma H, de Korne CM, Duszenko N, Langenberg MCC, Chevalley-Maurel SC, Smits HH, de Jong EC, Everts B, Franke-Fayard B, Roestenberg M. Plasmodium sporozoites induce regulatory macrophages. *PLoS Pathog*. 2020;16(9):e1008799. doi: 10.1371/journal.ppat.1008799. PubMed PMID: 32898164; PMCID: PMC7500643.
39. Cooney LA, Gupta M, Thomas S, Mikolajczak S, Choi KY, Gibson C, Jang IK, Danziger S, Aitchison J, Gardner MJ, Kappe SH, Wang R. Short-lived effector CD8 T cells induced by genetically attenuated malaria parasite vaccination express CD11c. *Infect Immun*. 2013;81(11):4171-81. doi: 10.1128/IAI.00871-13. PubMed PMID: 23980113; PMCID: PMC3811835.

40. Doerschuk CM, Beyers N, Coxson HO, Wiggs B, Hogg JC. Comparison of neutrophil and capillary diameters and their relation to neutrophil sequestration in the lung. *J Appl Physiol (1985)*. 1993;74(6):3040-5. doi: 10.1152/jappl.1993.74.6.3040. PubMed PMID: 8366005.

41. Noe A, Datoo MS, Flaxman A, Husainy MA, Jenkin D, Bellamy D, Makinson RA, Morter R, Ramos Lopez F, Sheridan J, Voukantsis D, Prasad N, Hill AVS, Ewer KJ, Spencer AJ. Deep Immune Phenotyping and Single-Cell Transcriptomics Allow Identification of Circulating TRM-Like Cells Which Correlate With Liver-Stage Immunity and Vaccine-Induced Protection From Malaria. *Front Immunol*. 2022;13:795463. doi: 10.3389/fimmu.2022.795463. PubMed PMID: 35197971; PMCID: PMC8859435.

42. Roozen GVT, van Schuijlenburg R, Hensen ADO, Koopman JPR, Lamers OAC, Geurten FJA, Sijtsma JC, Baalbergen E, Janse JJ, Chevalley-Maurel S, Naar CM, Bezemer S, Kroeze H, van de Stadt HJF, de Visser B, Meij P, Tihaya MS, Colstrup E, Iliopoulou E, de Bes-Roeleveld HM, Wessels E, van der Stoep M, Janse CJ, Murugan R, Franke-Fayard BMD, Roestenberg M. Single immunization with genetically attenuated PfΔmei2 (GA2) parasites by mosquito bite in controlled human malaria infection: a placebo-controlled randomized trial. *Nat Med*. 2025. doi: 10.1038/s41591-024-03347-2. PubMed PMID: 39753962.

Supplementary Data

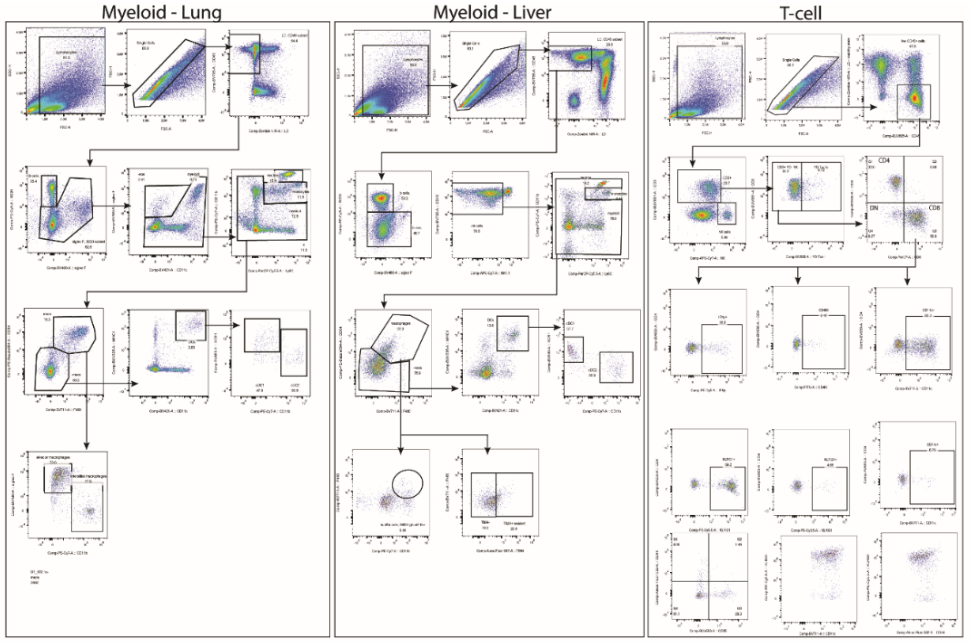

Supplemental Figure 1. Gating strategy. Gating strategy used to gate out liver and lung myeloid cells. Same gating strategy is used for the different experiments. All gating was performed in FlowJo.

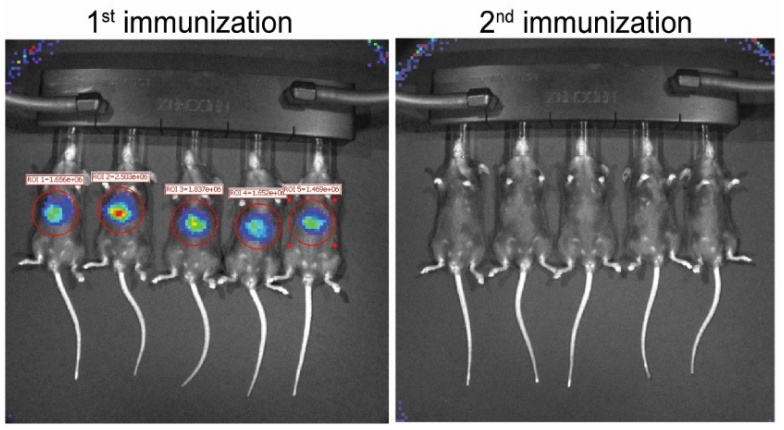

Supplemental Figure 2. liver load. Measurement of parasitic liver load by the expression of luciferase 44 hours after 1st immunization (left panel) and after 2nd immunization (right panel) with LA-GAP SPZ.

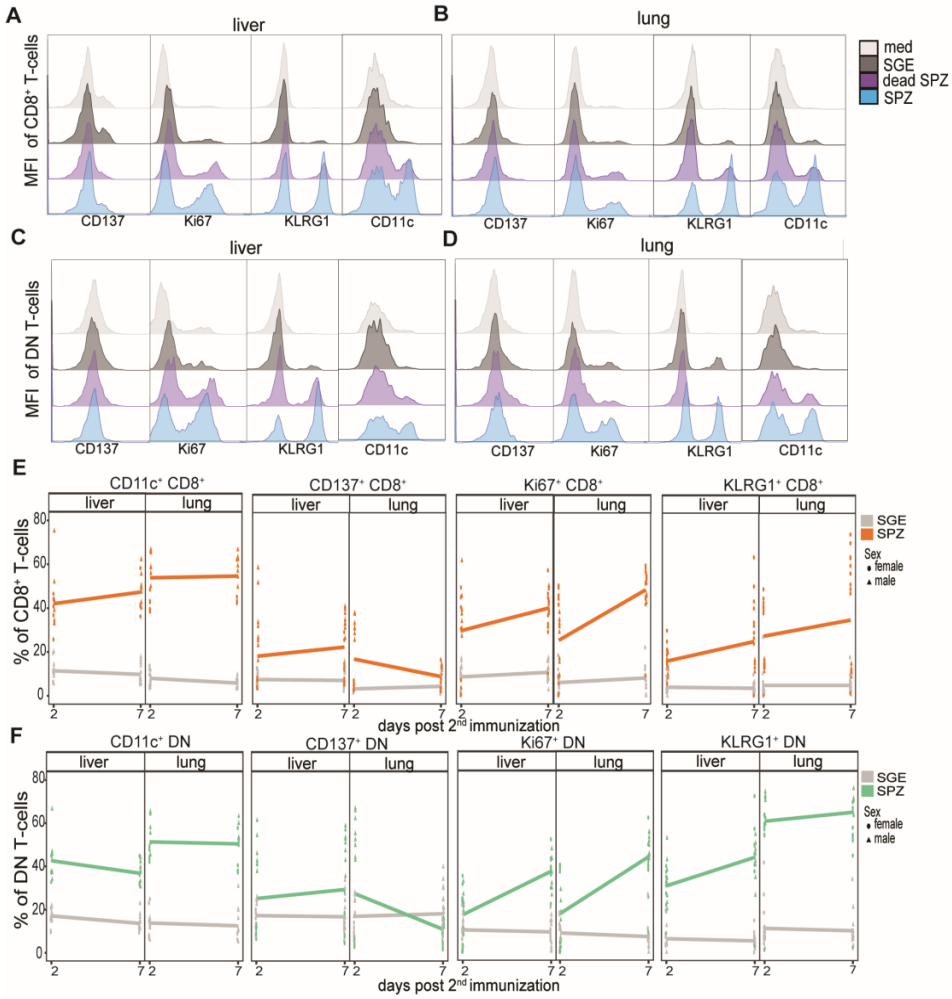

Supplemental Figure 3. Activation CD8⁺ T-cells and DN T-cells histograms and expression over time. (**A**) Histogram of Medium Fluorescence intensity (MFI) of different markers on CD8⁺ T-cells in the liver. (**B**) Histogram of MFI of different markers on CD8+ T-cells in the lungs. (**C**) Histogram of MFI of different markers on DN T-cells in the liver. (**D**) Histogram of MFI of different markers on DN T-cells in the lungs. Med in grey, SGE in grey, dead SPZ in purple, SPZ in blue. (**E**) Percentage of different activation markers on CD8⁺ T-cells over time (from 2 to 7 days after last immunization) in liver and lungs. SGE injected mice in grey, SPZ injected mice in orange. (**F**) Percentage of different activation markers on DN T-cells over time (from 2 to 7 days after last immunization) in liver and lungs. SGE injected mice in grey, SPZ injected mice in green. Med n=14, SGE n=18, dead SPZ n=10, SPZ n=18, divided over 2 (dead SPZ) or 3 (med, SGE, SPZ) experiments. Male mice in triangles and female mice in circles.

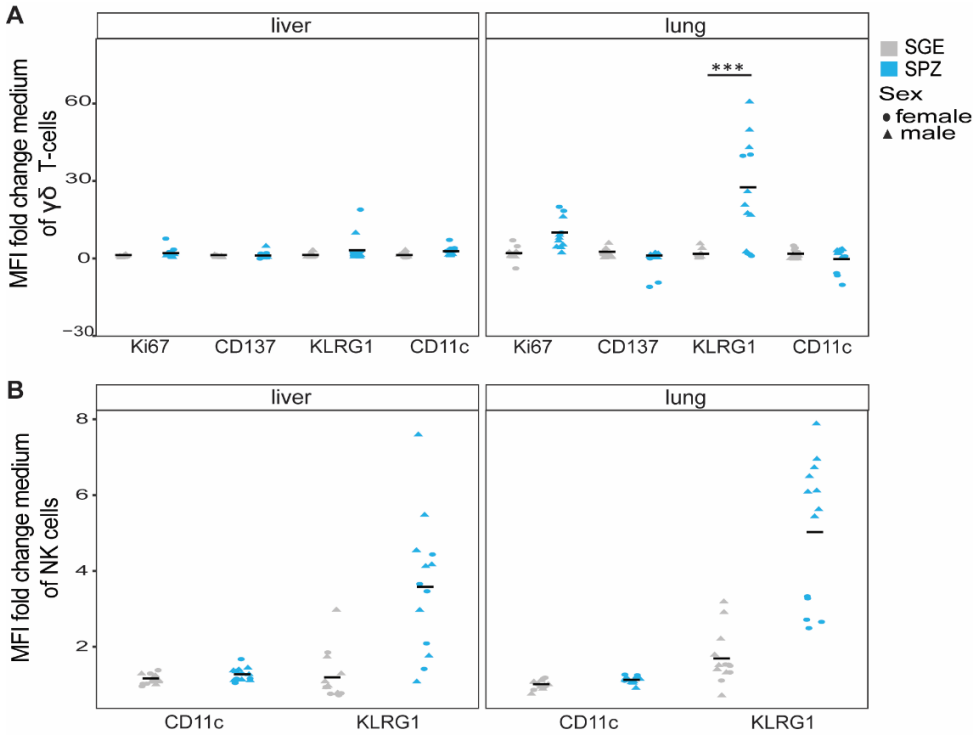

Supplemental Figure 4. Cellular activation γδ T-cells and NK-cells. Medium Fluorescence intensity (MFI) of different markers used to calculate fold change compared with medium (med). For the med group, mean of all mice per experiment was used. (**A)** Expression of different markers on γδ T-cells in the liver and lungs. (**B)** Expression of different markers on NK cells in the liver and lungs. In grey salivary gland extract (SGE) injected mice and in blue sporozoite (SPZ) injected mice. Med n=14, SGE n=18, dead SPZ n=10, SPZ n=18, divided over 2 (dead SPZ) or 3 (med, SGE, SPZ) experiments. Male mice in triangles and female mice in circles. Statistical significance between groups was assessed by one-way ANOVA with multiple comparisons. *: P=<0.05, **: P= <0.005, ***: P=<0.0005 and ****: P=<0.0001.

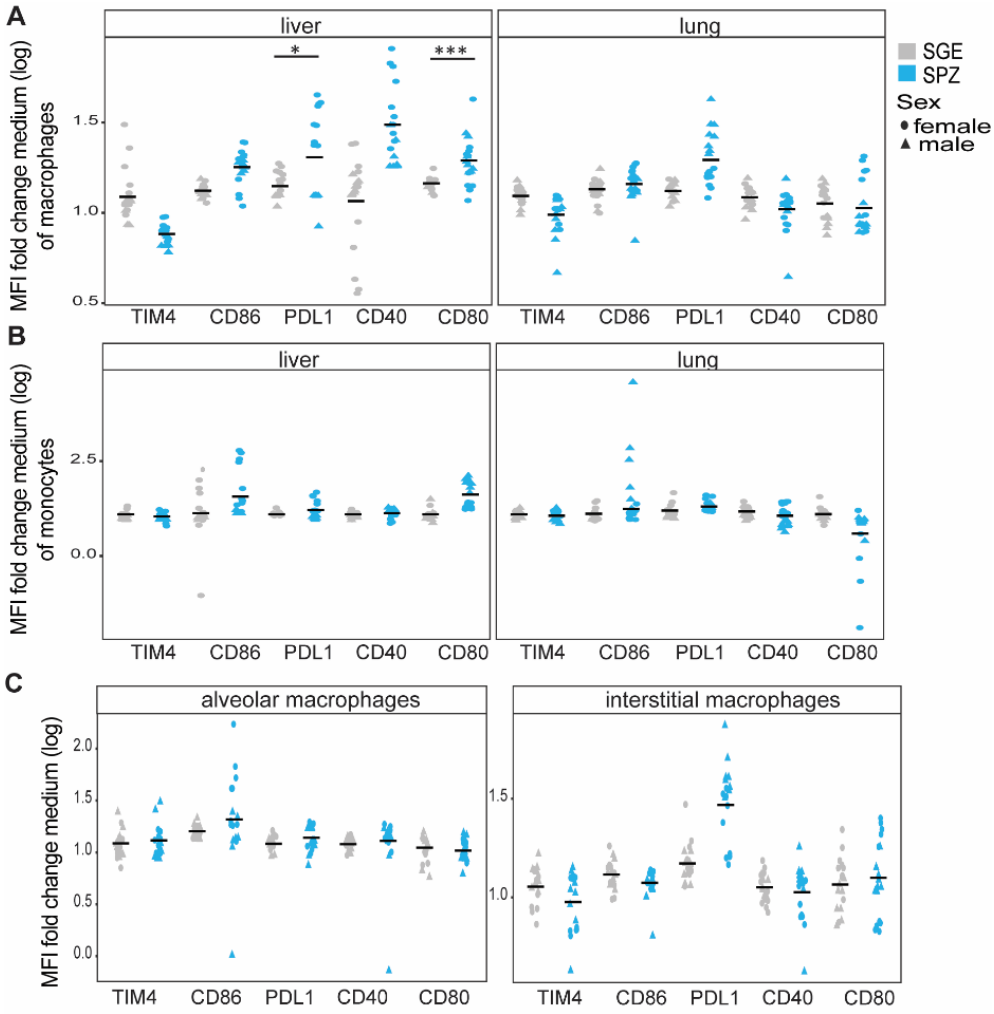

Supplemental Figure 5. Cellular activation myeloid and B-cells. Medium Fluorescence intensity (MFI) of different markers used to calculate fold change compared with medium (med). For the med group, mean of all mice per experiment was used. (**A)** Expression of different markers on macrophages in the liver and lungs. (**B)** Expression of different markers on monocytes in the liver and lungs. (**C)** Expression of different markers on alveolar and interstitial macrophages in the lungs. In grey salivary gland extract (SGE) injected mice and in blue sporozoite (SPZ) injected mice. Med n=14, SGE n=18, dead SPZ n=10, SPZ n=18, divided over 2 (dead SPZ) or 3 (med, SGE, SPZ) experiments. Male mice in triangles and female mice in circles. Statistical significance between groups was assessed by one-way ANOVA with multiple comparisons. *: P=<0.05, **: P= <0.005, ***: P=<0.0005 and ****: P=<0.0001.

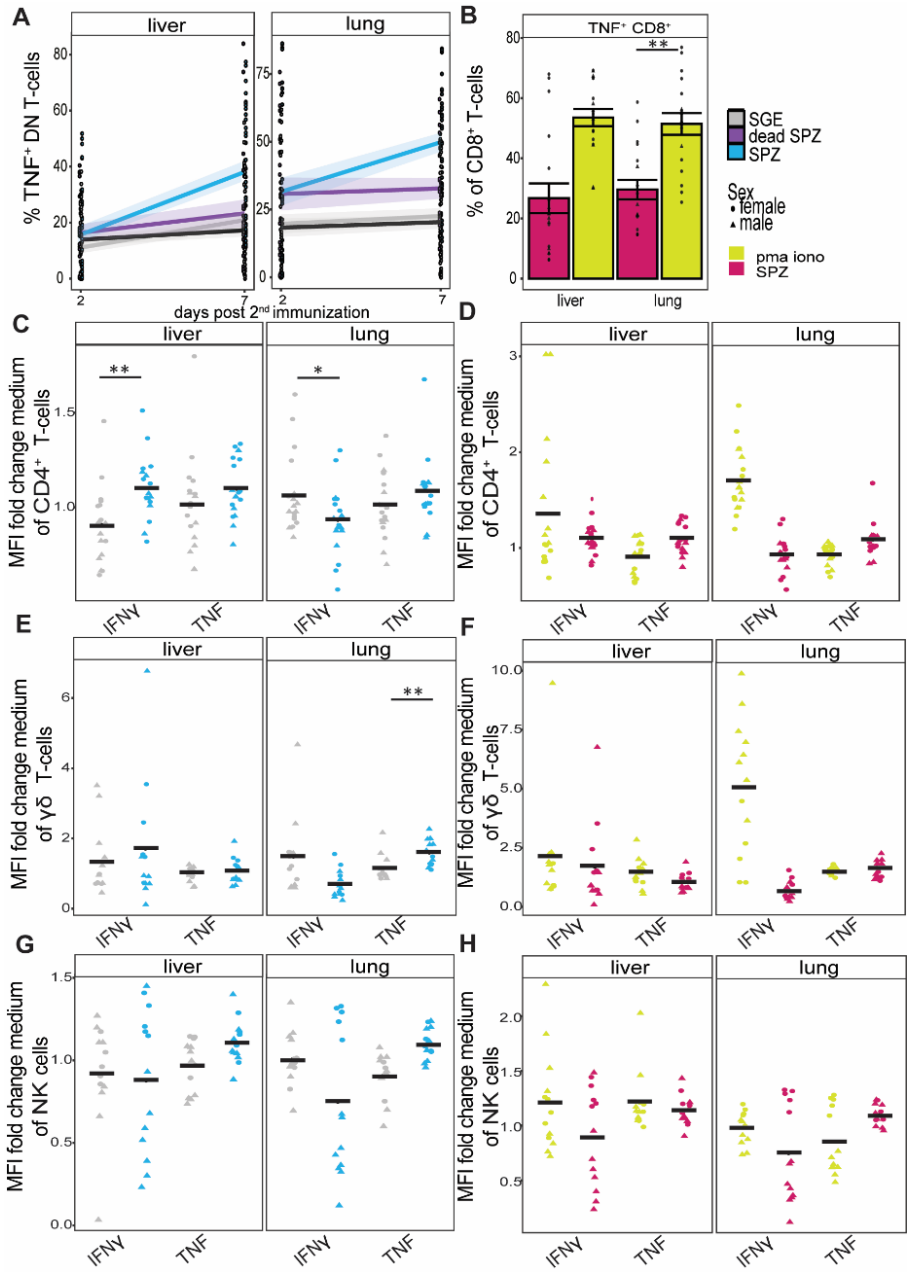

Supplemental Figure 6. Cytokine expression. (**A**) Percentage of TNF^{+} DN T-cells over time (time (from 2 to 7 days after last immunization) in liver and lungs. Med in grey, SGE in grey, dead SPZ in purple, SPZ in blue. (**B**) Percentage of TNF^{+}CD8^{+} T-cells after PMA/Iono restimulation (yellow) or SPZ restimulation (pink) at 7 days after SPZ immunization in liver and lungs. (**C**) Fold change compared with medium expression of IFNγ and TNF on CD4^{+} T-

cells in the liver and lungs after SGE (grey) or SPZ (blue) immunization. (**D**) Fold change expression of IFNγ and TNF on CD4+ T-cells after PMA/Iono (yellow) or SPZ (pink) restimulation in the liver and lungs compared with medium. (**E**) Fold change expression of IFNγ and TNF on γδ T-cells in the liver and lungs after SGE (grey) or SPZ (blue) immunization compared with medium. (**F**) Fold change expression of IFNγ and TNF on γδ T-cells after PMA/Iono (yellow) or SPZ (pink) restimulation in the liver and lungs compared with medium. (**G**) Fold change expression of IFNγ and TNF on NK cells in the liver and lungs after SGE (grey) or SPZ (blue) immunization compared with medium. (**H**) Fold change expression of IFNγ and TNF on NK cells after PMA/Iono (yellow) or SPZ (pink) restimulation in the liver and lungs compared with medium. Medium Fluorescence intensity (MFI) of different markers used to calculate fold change compared with medium (med). For the med group, mean of all mice per experiment were used. Med n=14, SGE n=18, dead SPZ n=10, SPZ n=18, divided over 2 (dead SPZ) or 3 (med, SGE, SPZ) experiments. Male mice in triangles and female mice in circles. Statistical significance between groups was assessed by one-way ANOVA with multiple comparisons. *: P=<0.05, **: P= <0.005, ***: P=<0.0005 and ****: P=<0.0001.